Struct Multidisc Optim (2010) 41:1–15
DOI 10.1007/s00158-009-0410-4

RESEARCH PAPER

Optimization of near-constant force springs subject to mating uncertainty

John C. Meaders · Christopher A. Mattson

Received: 9 January 2008 / Revised: 27 May 2009 / Accepted: 11 June 2009 / Published online: 11 July 2009

Abstract Constant force mechanisms are mechanical devices that provide a near-constant output force over a sizable and prescribed deflection range. These mechanisms have proven to be innovative solutions in a variety of applications. This paper considers a new application – the robust design optimization of constant force electrical contacts. Electrical contacts are inexpensive, small-scale, springs that carry electrical current. To produce these contacts at competitively low manufacturing costs, expensive pin-joints (a principle component of traditional kinematic mechanisms) are replaced by simple cam followers. Under certain conditions, enforced in this paper, cam followers can be used to emulate traditional pin-joints, and achieve the necessary motion. These emulated pin-joints, however, are subject to mating/assembly uncertainties that affect performance and must be considered in the design. In this paper, a numerical optimization model is used to characterize the force-deflection relationships for both an exactly mated emulated pin-joint, and for one that is subject to mating uncertainties. The numerical results show that under the exact mating conditions, a contact with 97.50% constant force can be identified (an improvement of 24.3% over previously published results), albeit sensitive to mating uncertainty. When conditions are considered uncertain, a more robust design is found with a 98.20% constant force. These surprising results are described in detail and verified with Monte Carlo simulation to confirm the results.

J. C. Meaders · C. A. Mattson (✉)
Department of Mechanical Engineering,
Brigham Young University, Provo, UT 84602, USA
e-mail: mattson@byu.edu

Keywords Constant force mechanism · Non-linear finite element analysis · Multiobjective optimization · Robust design optimization · Electrical contact

Nomenclature

α_c	Smallest angle between the cam link and the preceding element before deformation
γ_c	Smallest angle between the cam link and the preceding element after deformation
α_i	Smallest angle between the i-th element and the $i+1$ element
$\beta_{\max}$	Maximum transmission angle that the optimization search allows between the cam and the preceding element
C	Percent constant force
Δ	Total deflection (prescribed)
δ_p	Preload deflection
δ	An increment of the total prescribed deflection Δ
d_{ij}	Minimum distance between the i-th element and the jth element
F	Output force
Γ_x	Size of the design domain in x direction
Γ_y	Size of the design domain in y direction
L_i	Length of the i-th element
N	Safety Factor on Stress
n_n	Number of nodes
n_e	Number of elements
p	Vector of designer specified parameters
ψ	Minimum angle allowed between the cam link and the vertical and horizontal positions
θ_c	Angle of the cam link as measured from the horizontal
R_i	Distance from the i-th node to the cam center

r_c Radius of the cam
$\sigma_{\max}$ Maximum Bending Stress
x Vector of nodal coordinates in x direction
y Vector of nodal coordinates in y direction
Y_s Yield Strength

1 Introduction

From time to time, designs would benefit from having springs that exhibit a near-constant output force over a sizable, and prescribed, displacement range. These springs, whose force-displacement curves are notably different than linear springs, are referred to as constant force springs (Weight et al. 2007).

The constant force springs considered in this paper are derived from a broader class of constant force devices characterized as constant force kinematic mechanisms, which are modelled using traditional kinematic analysis (Howell 2001; Nahar and Sugar 2003; Evans and Howell 1999; Howell and Magleby 2006). While the constant force springs presented in this paper are kinematic mechanisms, they do not possess revolute joints (pin-joints). Instead, the necessary motion is obtained by (i) the large deflection of the spring's sections, and (ii) by simple cam followers, which can emulate the motion of a revolute-joint. These cam followers are described shortly, and are hereafter referred to as *emulated pin-joints*.

In this paper we present the design optimization of constant-force springs with emulated pin-joints and with consideration of uncertainty in the emulated pin-joint mating conditions. We specifically focus on the design of small scale (roughly 6 mm tall), mass produced electrical contacts, the basic architecture of which is shown in Fig. 1. The purpose of the electrical contact is to provide a reliable and separable electrical connection between two electrical devices. The constant force contact is designed to carry out that purpose with minimal variation in output force, which is a promising solution to common signal-integrity-difficulties encountered in separable electrical interconnections (Weight et al. 2007).

As illustrated in Fig. 1, the constant force contact assembly comprises (i) a plastic housing, and (ii) a metallic beam that is fixed at one end to the housing and makes contact with a plastic cam surface on the other. When the electrical connection is made, a device to which the connector mates applies a large displacement (labeled Input Deflection) to a point on the beam. This creates a reaction force (labeled Output Force) which is designed to be relatively constant over a large displacement range. The actual magnitude of

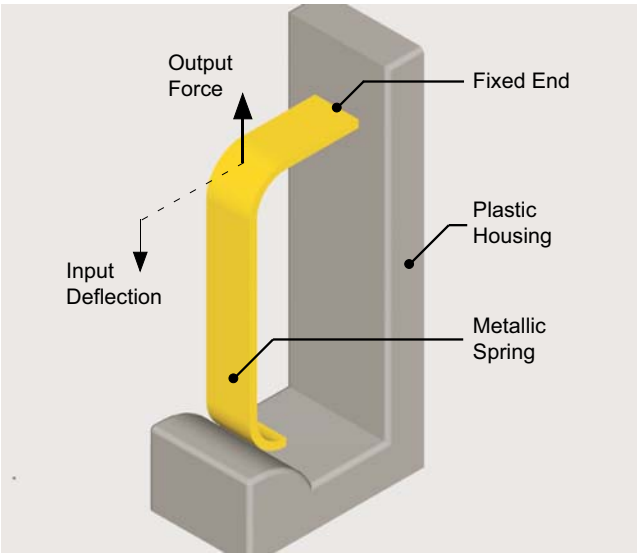

Fig. 1 Basic architecture of the compliant constant force electrical contact

displacement depends on several case-specific factors including the geometry and stiffness of both devices.

To produce these contacts at competitively low manufacturing costs, emulated pin-joints have been used in place of more expensive pin-joints. Under certain conditions, enforced in this paper, cam followers can be used to emulate traditional pin-joints, and achieve the necessary kinematics. Figure 2 illustrates the definition of an emulated pin-joint. As shown in the figure, the emulated pin-joint is located at the point where the metallic beam contacts the circular plastic cam. This connection, if maintained in compression, simulates a traditional pin-joint between the metallic beam and an imaginary rigid link connected to the cam center and having a length equal to the cam radius, r_c. These emulated joints, however, are subject to mating/assembly uncertainties that can significantly change the percent constant a mechanism's output force is, if not considered and handled explicitly. While extensive work has been done to predict the effect of uncertainty in traditional pin-joints (Garrett and Hall 1969; Choi et al. 1998) (by considering joint clearances), alternative models are needed that consider large mating gaps and large interferences between the compliant metal spring and the plastic cam.

As described in this paper, we seek robust designs that (i) exhibit a high constant force percentage, and (ii) are insensitive to mating/assembly uncertainties. Formally, a robust design can be defined as one whose performance remains relatively unchanged and feasible in the presence of uncertainty (Chen et al. 2000). Optimization-based robust design approaches seek to

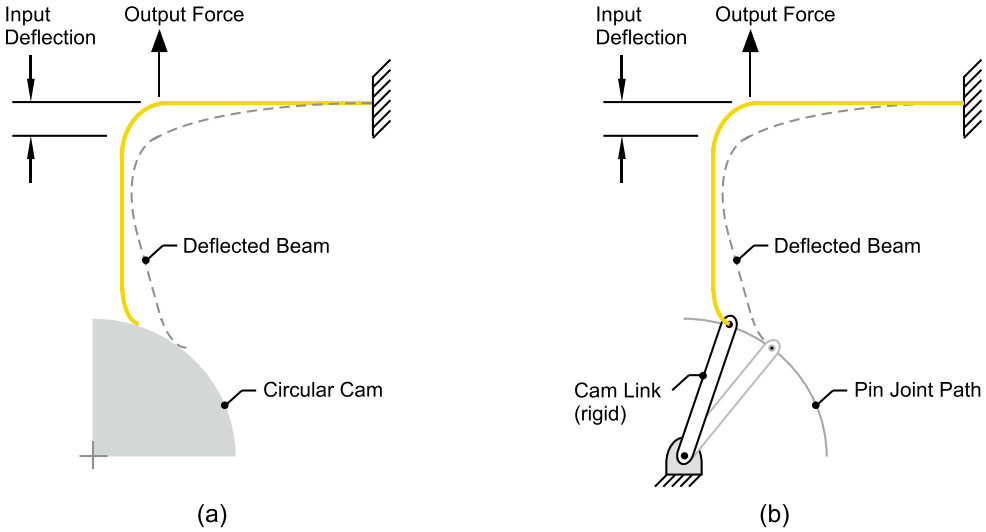

Fig. 2 Side view of basic constant force contact architecture; (**a**) Emulated pin-joint between beam and cam. (**b**) traditional pin-joint between beam and cam

optimize the mean performance and minimize its variation, while maintaining feasibility with probabilistic constraints (Taguchi 1986; DeVor et al. 1992; Koch 2002). The approach originates from Taguchi's theories on handling uncertainty in practice (Taguchi 1986). Noted work in this area includes Parkinson et al. (1993), and Chen et al. (1999, 2000). Su and Renaud (1997) provide an extensive review of the optimization-based robust design literature.

This paper presents a new design optimization approach for constant force springs. The approach can incorporate the uncertain nature of emulated pin-joints. Deterministic and robust design results are presented and compared to deterministic results published by Weight et al. (2007). As shown, the design approach presented here yields significant improvement over the previous study (Weight et al. 2007).

2 Technical preliminaries

Various developments have been made for the general modeling and design of constant force mechanisms (Jenuwine and Midha 1994; Herder and van den Berg 2000; Nathan 1985). Among the most useful developments is the Pseudo Rigid Body Model (PRBM); a method for designing *compliant* constant force mechanisms (Howell 2001). Compliant mechanisms gain some or all of their motion from the large deflection of flexible members as opposed to movement of rigid links connected by pin-joints. The PRBM is used to analyze compliant mechanisms as rigid-body mechanisms, thereby significantly reducing the complexity of analysis (Howell 2001; Evans and Howell 1999; Howell and Magleby 2006; Weight 2001).

One of the most common approaches for modeling a constant force mechanism is as a traditional slider crank mechanism with torsional springs at some or all of the joints (Murphy et al. 1996; Weight et al. 2002; Frischknecht et al. 2004). Such a mechanism is shown in Fig. 3a. The constant force behavior of this mechanism is due primarily to (i) the decreasing force transmission angle, from greater than $\pi/2$ to $\pi/2$, between the two long links in the figure, and (ii) the increasing spring force as the torsional spring deflects. To design constant force mechanisms based on this model, a designer must

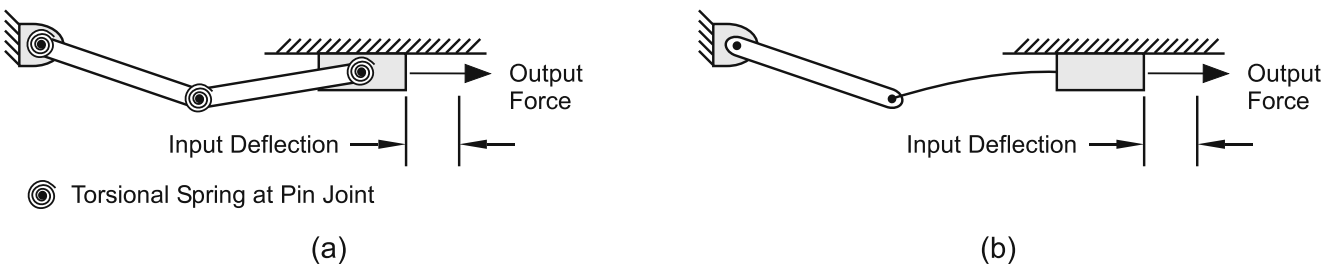

Fig. 3 (**a**) Compression-type constant force mechanism with rigid links and torsional springs at pin-joints. (**b**) One configuration of a compliant constant force mechanism with flexible and rigid links

select geometry, and torsional spring constants that balance the decreasing transmission angle and the increasing spring force (Parkinson et al. 1997). Figure 3b shows a compliant constant force mechanism. Here, the decreasing transmission angle must be balanced with increasing strain energy in the flexible link in order to achieve constant force behavior.

In a previous publication, we presented a constant force electrical contact that was based on the slider crank model and was identified using a deterministic optimization approach (Weight et al. 2007). We discussed the challenges with using the slider crank model to represent the compliant electrical contact, and presented solutions to overcome them. These challenges were largely related to using emulated pin-joints in place of traditional pin-joints. The problems identified included avoiding inflection points, tension at the emulated joint, friction, and deflection beyond a tangent point on the cam. The developments in the publication (Weight et al. 2007) did not include a discussion on, or remedy to, handling uncertainty associated with emulated pin-joint assembly and mating, which is the key component of the present paper.

As part of the study by Weight et al., a proof-of-concept prototype was manufactured and tested. The prototype is shown in Fig. 4. After an initial preload of 0.15 mm (20% of the total deflection), the prototype was 71.89% constant over the remaining 0.60 mm. Importantly, the prototype performed as predicted by the optimization routine, which was only able to find a design that was 73.20% constant. One of the most important observations made during the testing of these prototypes was that the performance of the samples was highly sensitive to mating conditions between the metal contact and the plastic cam.

In the present paper, we describe a new geometric layout (still based on the slider crank model) for the constant force contact and present a new optimization problem statement that (i) optimizes the percentage of constant output force, above that which was found in our previous work, and (ii) includes the effect of uncertainty, to the extent that the results presented in this paper have less variation in output force compared to previous work (Weight et al. 2007).

3 Constant force spring model and optimization

In this section we present a strategy and associated models for the design and optimization of small scale (roughly 6 by 6 mm) compliant constant force springs. We make the reasonable assumption that constant force springs can be modeled two dimensionally, with a prescribed and constant out-of-plane depth. We also assume that the constant force spring is formed from initially straight stock material through common manufacturing methods such as progressive-die forming. Our design strategy, therefore, is to execute an optimization search for two-dimensional spring shapes that can be formed in a progressive die and that exhibit constant force behavior. The variables in the optimization search are the nodal locations of principle bends in the spring geometry, (x_i, y_i), the location of the cam center, (x_c, y_c), and the cam radius, r_c. The following sections define the design domain, mating uncertainty, the constant force spring model, and deterministic and robust design optimization formulations for compliant constant force springs.

3.1 Design domain model

Figure 5 depicts the design domain – the shaded space within which the optimization searches for desirable contact shapes (dimensions: Γ_x by Γ_y). The geometry of the contact is represented by straight beam elements (shown as dashed lines) connected at nodes (x_i, y_i) as shown in the figure. A clamped condition is imposed at point (x_o, y_o), where the spring is fixed to the plastic

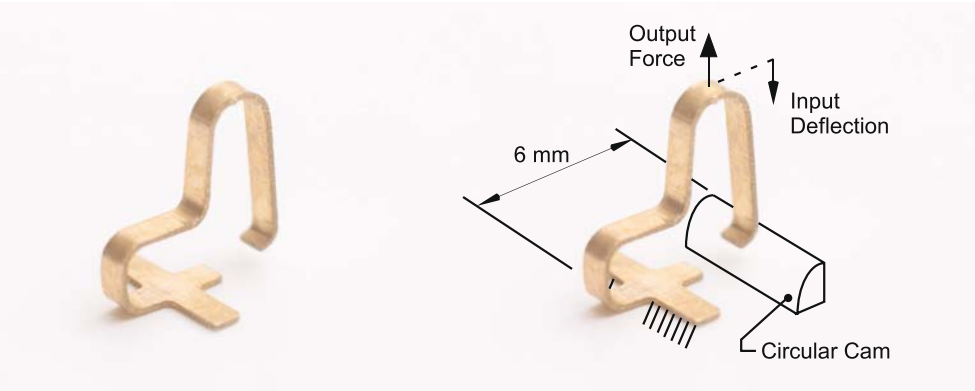

Fig. 4 Prototype resulting from the study by Weight et al. (2007)

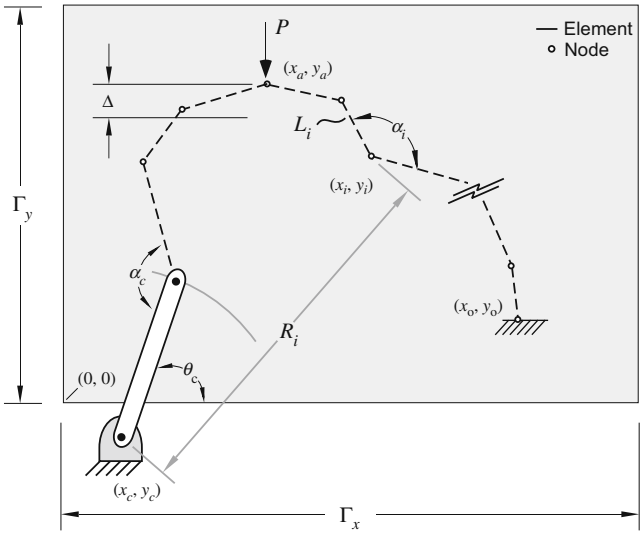

Fig. 5 Design domain and associated variables and parameters

housing. The geometry of the cam is depicted as a rigid kinematic link extending from the cam center (x_c, y_c) to the free end of the formed spring. Under the deterministic model, the free end of the cam link and the free end of the beam are constrained to occupy the same location; in other words, two nodes in the finite element model occupy the same spatial location. Additionally, with the no restriction on relative rotation between the cam link and the beam, these conditions characterize a kinematic pin-joint. All nodes, except the cam center (x_c, y_c), are constrained to be within the shaded design domain. Importantly, we note that allowing the cam center location (x_c, y_c) to be outside the shaded design domain brings additional freedom not present in previous work (Weight et al. 2007). Since the cam link is solely used in simulation (i.e., not manufactured), only the portion of the cam that contacts the spring from initial to final displacement is restricted to the design domain.

Figure 5 also shows a prescribed deflection (Δ) applied to a point (x_a, y_a) on the spring, and a reaction force (P), which is determined in the vertical direction. While the point (x_a, y_a) is subject to a prescribed deflection in the vertical direction, it is not constrained in the horizontal direction. The total number of nodes (n_n) and elements (n_e) in the design is chosen according to the desired resolution of the finite element model.

Unlike the geometric model from our earlier work (Weight et al. 2007), the present design domain model uses the Cartesian coordinates of each node (x_i, y_i) as variables for the design optimization. Because the nodal coordinates are permitted to be anywhere within the design domain, the optimization has nearly complete freedom to search for spring shapes that provide constant reactionary forces over large displacement ranges.

Figure 5 also illustrates variables that are used to formulate behaviorial constraints that ensure that the resulting design will be both manufacturable, and within the predictive capabilities of the emulated pin-joint model. Specifically, we define the angle between two adjacent elements (α_i), the length of each element (L_i), the distance from each node to the cam center (R_i), the angle between the cam link and the preceding element (α_c), and the angle (θ_c) of the cam link as measured from the horizontal. Each of these quantities is dependent on the nodal locations, which are independent variables. The behaviorial constraints that rely on these dependent variables are described shortly.

3.1.1 Geometric uncertainty model

When, at an undeflected spring state, it is assumed that the end of the spring is in perfect contact with the cam (i.e., no mating gap, and no strain in the spring), the search for desirable spring shapes can be carried out in a deterministic way. However, when the more realistic condition of mating gaps or initial strain in the spring is considered, a non-deterministic approach is needed. This section describes the geometric uncertainty model used to capture these non-deterministic effects.

The geometric uncertainty model presented here includes two sources of uncertainty. One source of uncertainty arises from manufacturing variations in spring shape, and by variations in other parameters such as material properties. The other source of uncertainty arises from imperfect mating conditions in the emulated pin-joint. To characterize the robustness of a particular design with respect to variation in manufacturing variables and other parameters we use a Monte Carlo simulation to create a population of contacts with normally distributed values for the spring's nodal locations. For each spring in the population, the percentage of constant force is determined. The standard deviation of the constant force percentages across the population determines the degree to which a design is robust.

Considering the second source of uncertainty, there are several different mating conditions that may be experienced between the assembled parts (metallic beam and plastic cam). Possible mating scenarios are illustrated in Fig. 6. The first case (Fig. 6a) is an ideal case where the beam and the cam mate exactly as designed – inducing no strain and leaving no gap. In this case, a deterministic search is sufficient. The second case (Fig. 6b) occurs when the cam is manufactured with a smaller radius than the design target. This results in a

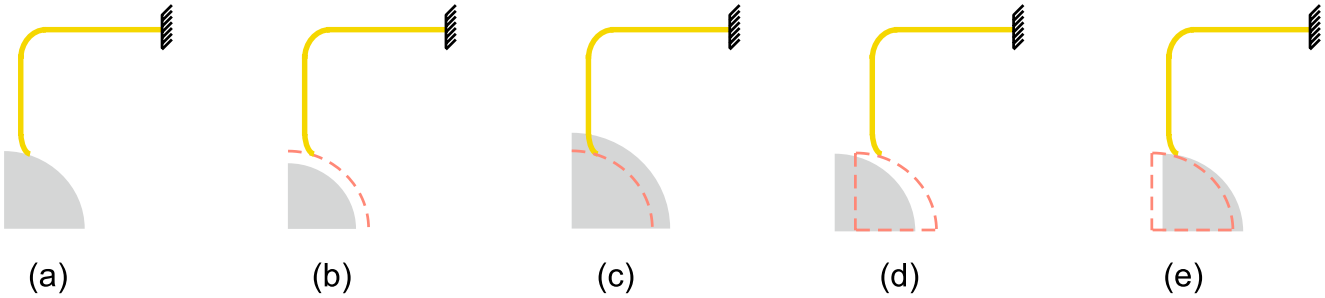

Fig. 6 Significant geometric uncertainties for emulated pin-joints. (**a**) Ideal case, (**b**) Cam radius too small, (**c**) Cam radius too big, (**d**) Cam and contact not fully assembled, (**e**) Cam and contact over assembled

gap between the cam and the beam, and the interaction between the two will not occur until the deflection of the beam closes this gap. The third case (Fig. 6c) occurs when the manufactured cam radius is larger than the design target. In this case, the cam will deflect the beam during assembly, induce strain in the spring, and cause the spring behave differently than expected. The fourth (Fig. 6d) and fifth (Fig. 6e) cases both involve variations in cam placement. For both cases, the cam and beam geometry are exact, however in Case 4 the contact is not fully assembled to the cam, which results in a gap. In Case 5, the contact is over assembled which causes the cam to deflect the spring during assembly – leaving a residual strain in the spring. All mating cases can be categorized into three basic conditions: an exact mating, a mating gap, or a mating interference.

To include the basic mating conditions in our analysis, we enhance the design domain model described above to include contact mechanics. For a constant force spring that has a gap between the spring and the cam, we enhance the design domain model by (i) removing the condition that the end of cam link and the end of beam occupy same location, and (ii) allowing the free end of the beam to move unconstrained until it contacts the cam surface. At each step of the multi-step load analysis, the size of the gap is tested to see if contact is made. When contact is made the pin-joint conditions are reactivated, meaning that the end of cam link and the end of beam are constrained to occupy same location, yet the links are free to rotate with respect to each other.

For a constant force spring that experiences a spatial interference between the spring and the cam, we enhance the design domain model by determining the deflection and stresses that are created by the interference – before applying the operational deflection. We do this by starting the cam in a position where the interference is removed and then applying several displacement steps to the cam center to move the cam back to its original position. This deflects the compliant member as if it was being assembled into the plastic housing. We use this deflected position and the corresponding residual stresses as our initial condition when we apply the total deflection.

Before discussing the methods used to determine the deflections and stresses in the designed spring, we pause to preview how these mating conditions are considered in the robust design optimization formulation described in Section 3.4. For each candidate design evaluated during the optimization search, the constant force characteristics of the design are examined for the nominal geometry, and for interference-generating geometry, and gap-generating geometry. These interference and gap generating geometries are invoked during the robust design optimization procedure. Additionally, a Monte Carlo simulation is performed on the final designs. In that simulation, thousands of interference and gap generating geometries are considered to evaluate the final design.

3.2 Modeling force-displacement and bending stress relationships

We use a finite element method to determine the force-deflection relationship of the spring, and to determine the internal stresses caused by the deflection. The overall spring geometry is modeled using a number of beam elements and the Timoshenko beam theory. This theory provides more accurate results than the Euler theory in beams with low length to thickness ratios. Since the length of each beam, and thus the length to thickness ratio, is decided by the optimizer, the Timoshenko beam theory is used to provide more accurate results.

The metallic spring undergoes large non-linear deflections. Therefore, nonlinear methods are used to solve the beam equations for nodal displacements. The non-linear finite element process, used in this paper, follows the procedures developed by Bhatti (2006). Bhatti suggests three main steps and the use of

Newton-Raphson approaches for solving the set of nonlinear equations. Step 1 is to form the global tangent stiffness matrix, the load vector, and the internal force vector through element assembly. Step 2 is to solve the system of equations for a small load step. Finally, Step 3 updates the nodal locations. Steps 1–3 are executed for each step of a multi-step load analysis.

We use a Newton-Raphson iteration method to converge on a nodal solution after providing an initial estimate of nodal displacements. The internal stresses and the reaction forces are calculated directly from the beam equations once the solution is known. One difficulty with the Newton-Raphson iteration is that it can diverge if the initial estimate is too far from the solution. To prevent this we apply the total deflection (Δ) to the contact in many small increments (δ).

These displacement increments, and the corresponding output forces, become data points for constructing the force-deflection curve. The force-deflection curves of constant-force contacts typically have a region where the force increases steeply with increasing deflection followed by a nearly flat region. A typical curve is shown in Fig. 7. As seen in the figure, a small preload is applied to avoid the region of steep force increase. This preload deflects the spring beyond the region of increasing force, so that the deflections that occur during operation are in the flat region. When determining the level of constant force for the contact we consider only the variation in force over the operational displacement range. Being consistent with previous literature (Weight et al. 2007; Howell 2001), the level or percentage of constant force is related to the maximum and minimum forces in that range by (1)

$$C = 100\frac{F_{\min}}{F_{\max}} \tag{1}$$

To avoid plastic deformation, the internal stresses must be determined. As the Newton-Raphson procedure is iterated the bending, axial, and shear stresses are estimated using the two dimensional beam equations. In this paper, however, we consider only the bending stress, as it is dominant. Failure is determined by comparing the bending stress to the material yield strength.

This section has presented the models used to characterize the performance of the constant force contact and the performance uncertainty due to variations in nodal locations and cam/beam mating (see Section 3.1). The following two sections use these models in optimization problems to identify contact geometry that results in constant force contacts.

3.3 Deterministic optimization formulation

In this section we present the deterministic optimization problem statement used to find optimal spring geometry that produces a constant force over a large prescribed deflection range. The constraints developed in this section are also used in the robust design optimization problem statement of Section 3.4, but will be

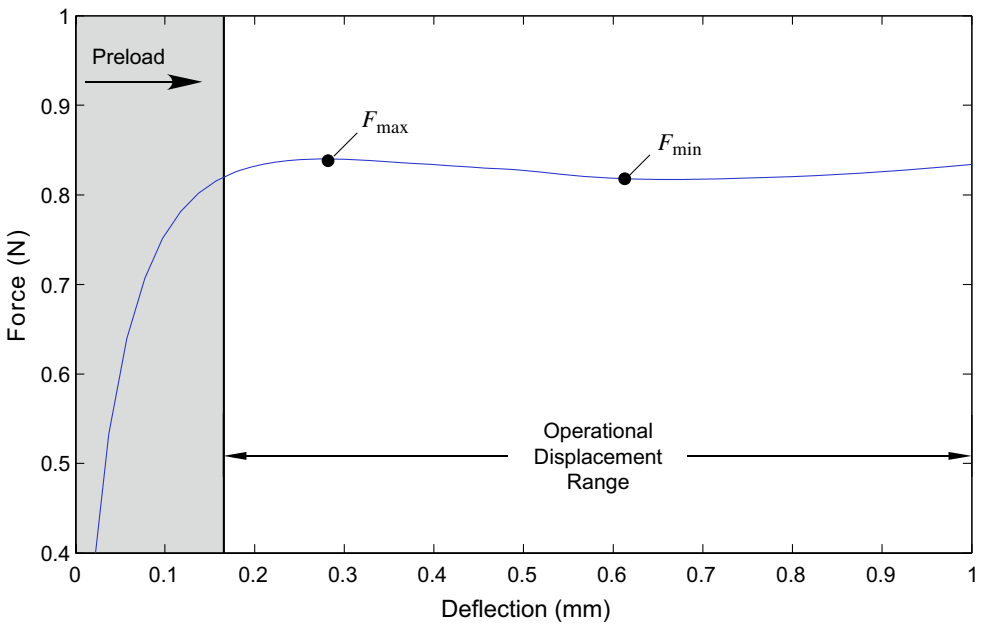

Fig. 7 Generic force-displacement curve for constant force device

altered to ensure that uncertain conditions do not lead to violated constraints.

Problem 1 Deterministic design optimization of the compliant constant force springs

$$\min_{x,y} \quad J_1 = \int_{\delta_p}^{\Delta} (F - F_{\text{ave}})^2 \, d\delta \tag{2}$$

subject to

$$F_L \leq F_{\text{ave}} \leq F_U \tag{3}$$

$$d_{ij} > 0 \qquad (i, j = 1, 2, ..., n_e, \, j > i + 1) \tag{4}$$

$$\alpha_i \geq \alpha_{\min} \qquad (i = 1, 2, ..., n_e - 1) \tag{5}$$

$$L_i \geq L_{\min} \qquad (i = 1, 2, ..., n_e) \tag{6}$$

$$\alpha_c \leq \beta_{\max} \tag{7}$$

$$\gamma_c \geq \frac{\pi}{2} \tag{8}$$

$$\frac{\pi}{2} - \psi \geq \theta_c \geq \psi \tag{9}$$

$$R_i \geq r_c \qquad (i = 1, 2, ..., n_n - 2) \tag{10}$$

$$r_{\max} \geq r_c \tag{11}$$

$$\sigma_{\max} \leq \frac{Y_s}{N} \tag{12}$$

$$0 \leq x_i \leq \Gamma_x \qquad (i = 1, 2, ..., n_n - 1) \tag{13}$$

$$0 \leq y_i \leq \Gamma_y \qquad (i = 1, 2, ..., n_n - 1) \tag{14}$$

where δ_p is the preload displacement, Δ is the total displacement, and F_{ave} is the average output force over the operational displacement range $(\Delta - \delta_p)$. The set of designer specified design parameters for this problem are listed in Table 1; and designer specified constraint limits are defined in Table 2. As seen by (2), the objective of this optimization problem is to minimize the difference in output force over a range of displacements, which maximizes the constant force percentage expressed in (1). A graphical representation of the objective function is presented in Fig. 8a. This figure shows a force-displacement plot and it's average force (dashed horizontal line) as evaluated over the operational displacement range. The objective function seeks to minimize the shaded area between the function F and F_{ave}. Equation (3) keeps the maximum output force below an upper limit and the minimum output force above a lower limit, for the forces encountered in the operational displacement range. Equation (4) is included in the problem statement to keep the string of elements from crossing over itself. We do this by constraining the minimum distance (d_{ij}) between any two *non*-adjacent elements to be greater than zero. Equations (5) and (6) limit the angle between adjacent elements and restricts the minimum length of the elements, respectively. These constraints are included in the statement to keep the search for constant force mechanisms practical from a manufacturing perspective. Equations (7) and (9) keep the cam link angles within the capabilities of the emulated pin-joint model, and (8) and (10) keep the nodes and elements of the contact from passing through the cam surface or trying to occupy any space where the cam physically exists. Stress is maintained under control by (12). Finally, the nodal locations, which are completely free to move during the optimization search, are required to stay within the design domain as specified by (13) and (14). Again, we note that the cam center, however, is allowed to move outside of the design domain. Notice when the indices used to define the constraints in (4)–(6), (10), (13), and (14), are expanded for a 17 element

Table 1 Parameter description for deterministic optimization

Parameter	Description
x_o	x coordinate of fixed point
y_o	y coordinate of fixed point
x_a	x coordinate of point where force is applied
y_a	y coordinate of point where force is applied
n	Number of nodes
E	Young's modulus
ν	Poisson's ratio
b	Cross section width
h	Cross section height
Δ	Total deflection range including preload

Table 2 Constraint limit descriptions

Parameter	Description
Γ_x	x dimension of design domain
Γ_y	y dimension of design domain
$r_{\max}$	Maximum allowable cam radius
$\alpha_{\min}$	Min. allowable angle between adjacent elements
$L_{\min}$	Minimum allowable element length
$\gamma_{\max}$	Smallest angle between cam link and preceding element after deformation
F_L	Minimum allowable output force
F_U	Maximum allowable output force
$\beta_{\max}$	Maximum allowable transmission angle between cam and the preceding element
ψ	Minimum allowable angle cam link and vertical and horizontal positions

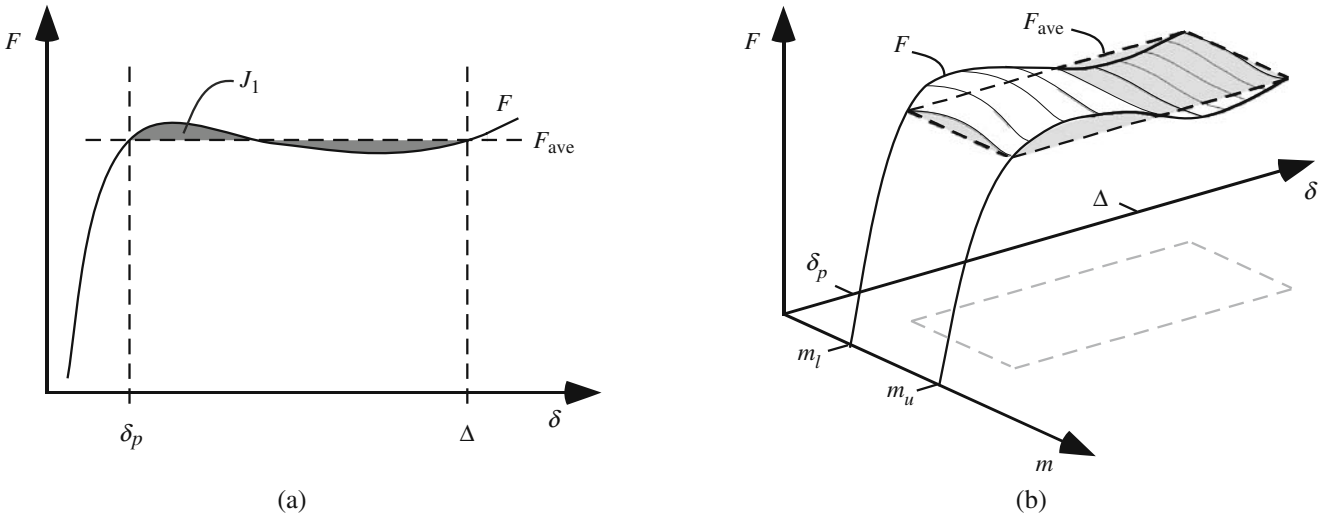

Fig. 8 (**a**) Area between the force-deflection plot and the average force is minimized over the operational displacement range, thereby maximizing the constant force percentage. (**b**) Volume between the force surface and the average force is minimized, thereby maximizing the constant force percentage over a range of mating conditions

constant force spring ($n_e = 17$), there are a total of 209 constraints.

3.4 Robust design optimization formulation

The optimization problem formulation presented in this section is used to search for optimal contact geometry that produces a near-constant force over the operational displacement range *and* decreases variation of that force given manufacturing related uncertainties.

Problem 2 Robust design optimization of the compliant constant force contact

$$\min_{x,y} \; J_2 = \int_{m_l}^{m_u} \int_{\delta_p}^{\Delta} (F - F_{\text{ave}})^2 \, d\delta dm \tag{15}$$

subject to

$$F_L + \tilde{F}_i \le F_{\text{ave}} \le F_U - \tilde{F}_i \tag{16}$$

$$d_{ij} > 0 + \tilde{d}_{ij} \qquad (i, j = 1, 2, ..., n_e, \; j > i + 1) \tag{17}$$

$$\alpha_i \ge \alpha_{\min} + \tilde{\alpha}_i \qquad (i = 1, 2, ..., n_e - 1) \tag{18}$$

$$L_i \ge L_{\min} + \tilde{L}_i \qquad (i = 1, 2, ..., n_e) \tag{19}$$

$$\alpha_c \le \beta_{\max} - \tilde{\alpha}_c \tag{20}$$

$$\gamma_c \ge \frac{\pi}{2} + \tilde{\gamma}_c \tag{21}$$

$$\psi + \tilde{\theta}_c \le \theta_c \le \frac{\pi}{2} - \psi - \tilde{\theta}_c \tag{22}$$

$$R_i \ge r_c + \tilde{R}_i \qquad (i = 1, 2, ..., n_n - 2) \tag{23}$$

$$r_{\max} \ge r_c + \tilde{r}_c \tag{24}$$

$$\sigma_{\max} \le \frac{Y_s}{\tilde{N}} \tag{25}$$

$$0 + \tilde{x}_i \le x_i \le \Gamma_x - \tilde{x}_i \qquad (i = 1, 2, ..., n_n - 1) \tag{26}$$

$$0 + \tilde{y}_i \le y_i \le \Gamma_y - \tilde{y}_i \qquad (i = 1, 2, ..., n_n - 1) \tag{27}$$

where F_{ave} is the average force over the operational displacement range *and* over the range of possible mating conditions (m_l to m_u). The terms m_l and m_u indicate the lower and upper mating conditions for the candidate design, respectively. Importantly, by simple geometric analysis, the range of mating conditions, and therefore m_l and m_u, can be calculated for any candidate design.

The objective function for Problem 2 is presented graphically in Fig. 8b. Here, the force function is shown as a surface, which is a function of displacement, δ, and mating condition (meaning quantity of mating interference or mating gap), m. The average value of that function over the range of m, and over the operational displacement range, is shown as a flat surface with dashed-line borders. The objective function seeks to minimize the volume between the force function and the average force. Such an objective function results in a maximizing of the constant force percentage, and a minimizing of force variation over a range of mating conditions.

As mentioned earlier, it becomes necessary to adjust the constraints to ensure that any contact within our tolerance window does not violate our constraints. Equations (16) to (27) show the adjusted form of the deterministic constraint equations. An additional term has been added to each constraint that reduces the design space by an amount (shown with a tilde) that is determined by the variance in each of the constrained values. Determining an appropriate value for tightening the constraints can be difficult due to the dependence of many constraints on the finite element analysis. For constraints that depend only on the geometry of the design the constraint can be adjusted directly since we know what geometry our tolerance window will permit. For example, we know what limits our tolerances will allow on element lengths so we can directly adjust our constraint on the minimum element length such that no design will violate this constraint within a tolerance window. For a constraint such as the maximum allowable stress, however, we do not know what effect the tolerance window may have on the stress within the compliant member, since it depends on the non-linear finite element analysis. In this case we run a Monte Carlo simulation on a design, prior to optimizing, to determine the variance of the constrained finite element analysis values within our manufacturing tolerance limits. We then use this information to estimate how much we must adjust the constraint during the optimization routine. Using this approach we must check the optimum design to ensure that none of the original, or unadjusted, constraints is violated through variation in our design. We also use a Monte Carlo simulation, outside of the optimization algorithm, to verify the performance of a sample of contacts within the tolerance limits of our optimum design.

For both the deterministic and the robust design approaches we use a sequential quadratic programming (SQP) optimization routine to find the optimal solution. While this search method is useful because of its efficiency in converging on an optimal solution, it cannot guarantee convergence on a global optimum. In application, various search methods can be used. As a note, the objective function is highly nonlinear over the design space due to the complexity of the geometric model. A discontinuity can occur if the gap between the cam and the beam is too large, and no contact is made. A suitable starting design is necessary that will avoid such discontinuities.

4 Numerical results

This section presents two examples that demonstrate the optimization models developed in this paper. We compare the results of these two examples and highlight differences in performance and robustness that occur as a result of the different objective functions. We also compare our results to the results obtained by Weight et al. (2007) and observe the improvements that can be gained by using the design optimization

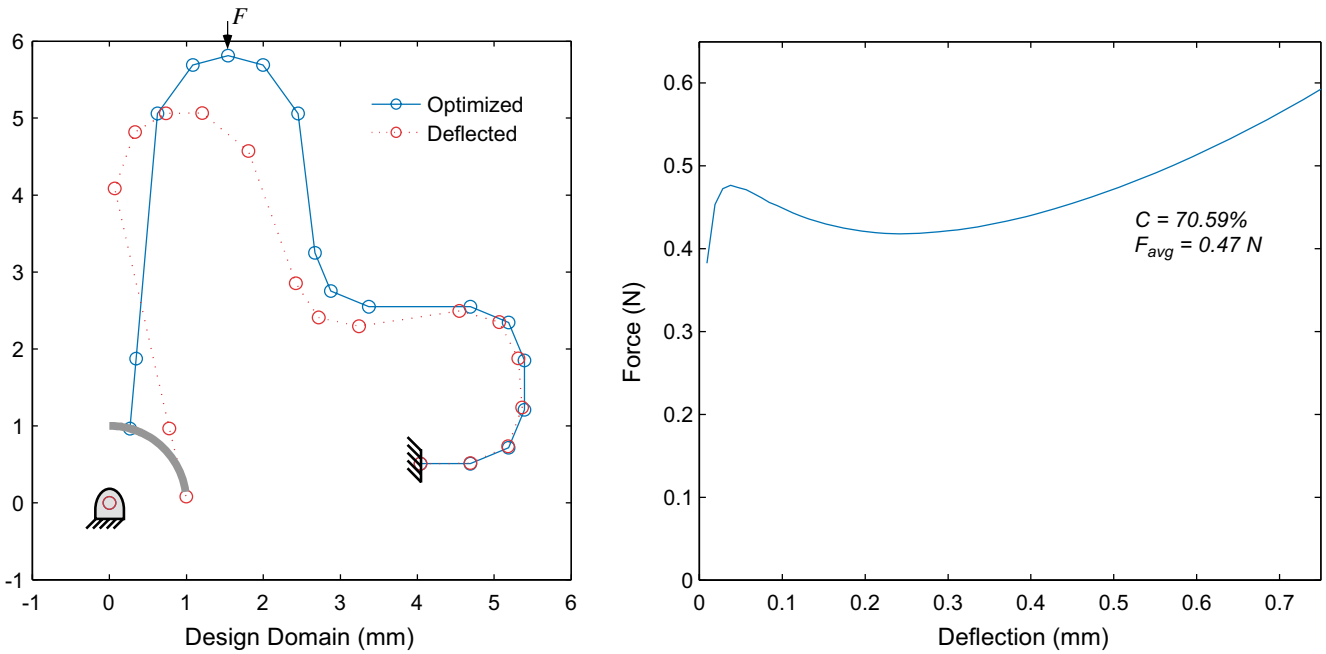

Fig. 9 Benchmark design: (**a**) Side view of optimized geometry with non-exaggerated deflected shape; (**b**) Force deflection curve

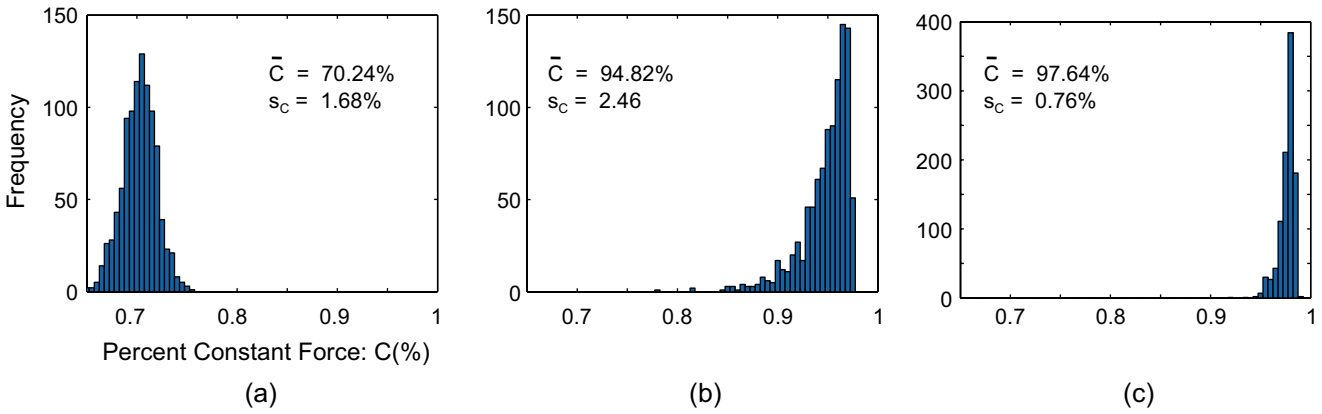

Fig. 10 Monte Carlo results for three designs with 1,000 samples each: (**a**) Benchmark design (**b**) Deterministic solution (**c**) Robust design solution

approach presented in this paper. For a complete comparison, the benchmark design, which was designed using the method presented in Weight et al. (2007), has been carefully approximated and analyzed using the approaches of the present paper. The results are shown in Figs. 9 and 10a. Figure 9 shows the side profile of the optimized geometry. When compared to the basic architecture shown in Fig. 1, it can be seen that the spring portions are metallic and fixed at one end, while the cam is plastic and makes contact with the free end of the spring.

4.1 Case 1: deterministic optimization and robustness check

The first example that we present is the design that results from the deterministic optimization statement. In this example we initially keep the assumption that the spring and the cam will maintain perfect contact. We then test this design by breaking the assumption and considering both sources of uncertainty discussed in Section 3.1 in a Monte Carlo simulation to observe how sensitive the design is to variation. Table 3 lists the fixed parameters used for this example. These values are selected to match the benchmark design (Weight et al. 2007), and all are in the range that could be considered when designing a constant-force-electrical contact for the electronics industry. We note that some terms described in Problem 2 are not listed in Table 3 (e.g., $\tilde{\alpha}$). This is because they are not fixed values, but instead vary with each spring geometry considered during the optimization process.

The resulting design in its undeflected and deflected state is shown in Fig. 11 with its corresponding force-deflection curve. The percentage of constant force for this design is 97.50% – a significant increase over our previous results Weight et al. (2007), which were reported as 73.2%. For the deterministic case, we attribute the improvement to two key factors: (i) The modeling approach for spring geometry used herein significantly, and strategically, opens the design space to geometries not available in the previous study. It does this by treating the location of the beam's principle

Table 3 Fixed parameter values for cases 1 and 2

Parameter	Description	Value
x_o	x coordinate of fixed point	4.04 mm
y_o	y coordinate of fixed point	0.51 mm
x_a	x coordinate of point where force is applied	1.54 mm
y_a	y coordinate of point where force is applied	5.81 mm
n	Number of nodes	18
E	Young's modulus	110 GPa
ν	Poisson's ratio	0.34
b	Cross section width	1.00 mm
h	Cross section height	0.2 mm
Δ	Total deflection range including preload	0.75 mm
δ_p	Preload deflection	0.11 mm
N	Safety factor on stress	1.0
$\tilde{x}$	Tolerance limit on x	0.03 mm
$\tilde{y}$	Tolerance limit on y	0.03 mm
$\tilde{E}$	Tolerance limit on E	5.0 GPa
$\tilde{\nu}$	Tolerance limit on ν	0.005
$\tilde{b}$	Tolerance limit on b	0.03 mm
$\tilde{h}$	Tolerance limit on h	0.03 mm
$\tilde{r_c}$	Tolerance limit on r_c	0.03 mm
$\tilde{L}$	Constraint shift needed for feasibility of L	0.06 mm
$\tilde{d}$	Constraint shift needed for feasibility of d	0.06 mm
$\tilde{R}$	Constraint shift needed for feasibility of R	0.06 mm

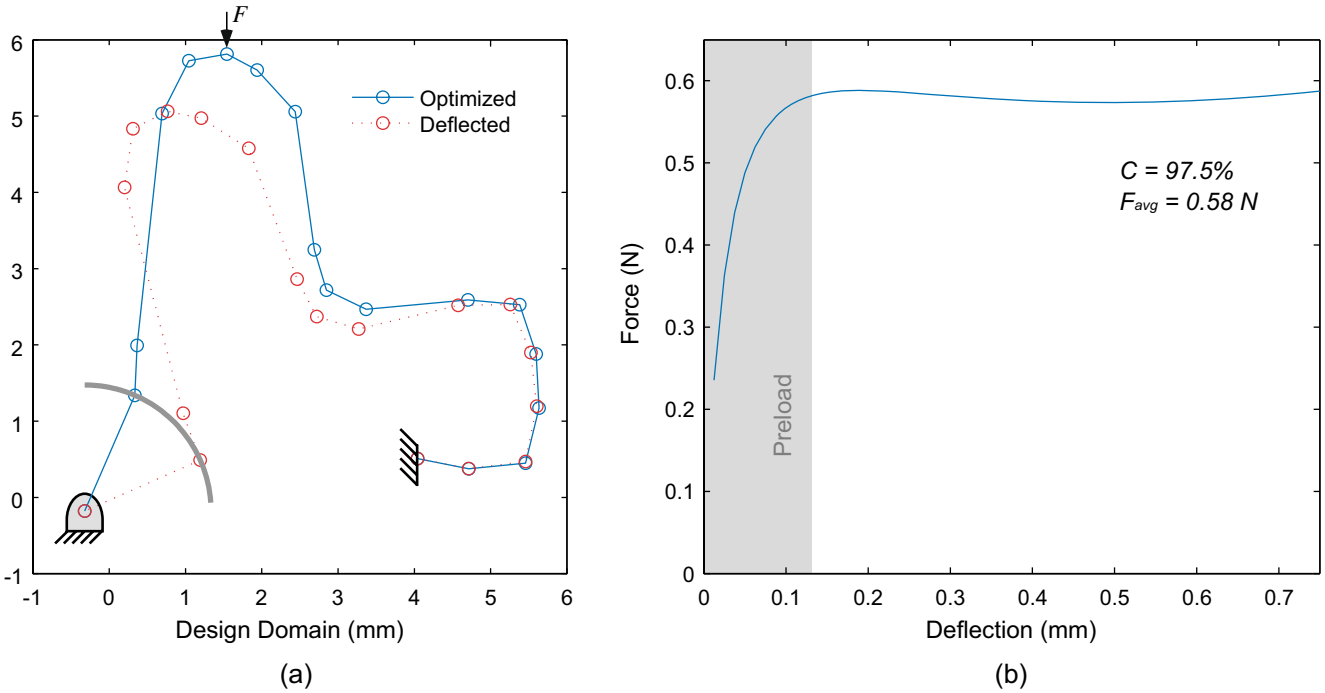

Fig. 11 Case 1 Deterministic solution: (**a**) Side view of optimized geometry (nodal representation) with non-exaggerated deflected shape; (**b**) Force deflection curve for optimized design

bends as design variables, and by allowing the location of the cam center to be outside of the design domain as long as the *useful* portion of the cam remains in the design domain. The useful portion of the cam is the area that contacts the spring over its full displacement. (ii) The constraints developed in the present study allow us to treat the location of the beam's principle bends as design variables *without* having the beam cross over, or wrap around, itself.

We now perform a Monte Carlo simulation on the design to determine the robustness of the results. In this simulation we will include uncertainty in all the design variables, and fixed values that we use for the finite element model. We also allow the mating condition to change depending on the random values of the other finite element inputs. For all the uncertain variables we use a normal distribution with a mean at the nominal value and a standard deviation equal to one third of the manufacturing tolerance, as obtained from industry collaborators, and shown in Table 3 and Table 4. Figure 10b shows the distribution of constant force percentages for a sample of 1,000 contacts. The average percentage for the sample is 94.82% constant with a standard deviation of 2.46%. The distribution of this sample is notably different than the distribution of the benchmark sample. This is explained by recognizing that an upper limit exists on the possible performance values for the samples ($C = 100\%$). As the nominal design performance approaches this limit, variations from the nominal design take on a skewed distribution because they cannot physically result in designs with $C > 100\%$. The next example reduces the standard deviation by implementing the robust design optimization.

We now make an important comment regarding the use of only 1,000 samples in the Monte Carlo simulation used post-optimization to establish robustness.

Table 4 Constraint limit values for cases 1 and 2

Parameter	Description	Value
Γ_x	x dimension of design domain	12 mm
Γ_y	y dimension of design domain	6 mm
$r_{\max}$	Maximum allowable cam radius	6 mm
$\alpha_{\min}$	Min. allowable angle between adjacent elements	100 deg
$L_{\min}$	Minimum allowable Element length	0.03 mm
$\gamma_{\max}$	Smallest angle between cam link and preceding element after deformation	175 deg
F_L	Minimum allowable output force	0.30 N
F_U	Maximum allowable output force	1.00 N
$\beta_{\max}$	Maximum allowable transmission angle between cam and the preceding element	175 deg
ψ	Minimum allowable angle cam link and vertical and horizontal positions	5 deg

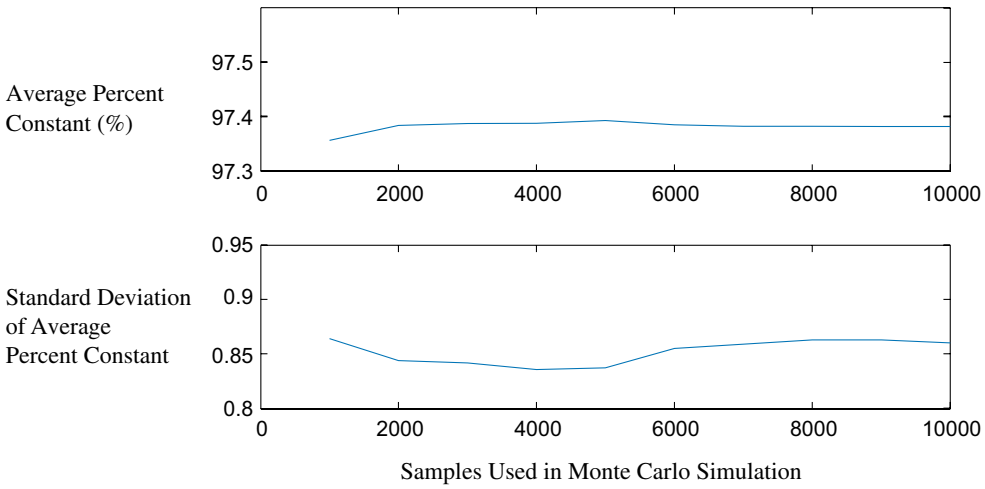

Fig. 12 Average percent constant (top) and standard deviation of average percent constant (bottom) over 10,000 Monte Carlo samples

For the design of a non-linear spring, such as the one considered in this paper, the computation time required to compute the non-linear finite element analysis is significant. We, therefore, use a small number of Monte Carlo samples, post optimization, to check the design's robustness. We do this, however, only after we have understood and accepted the error accompanying the Monte Carlo sample size. For the models used in this paper a plot of Average Percent Constant versus Samples used in Monte Carlo Simulation is plotted in Fig. 12. Also shown in the figure is a plot of the Standard Deviation as a function of samples in the Monte Carlo simulation. For both the constant force percentage (C) and the standard deviation thereof, it can be seen that 1,000 samples is a reasonable approximation of the same quantities as obtained with a larger number of samples.

4.2 Case 2: robust design optimization and robustness check

We now present an example in which we eliminate the assumption that the cam and the spring always stay in contact. We use the same designer specified parameters as Case 1, but in this case we use the robust design optimization approach as presented in this paper. Note that with the robust design approach we allow the optimizer to intentionally design a gap or an interference between the spring and the cam.

Figure 13 shows the resulting design's geometry with the nominal mating condition and the corresponding force deflection curve. The constant force percentage for this design is 98.20%. It may seem surprising that this percentage is higher than the deterministic solution since we have tightened the constraints and added two new objectives (C_L, C_U) to the formulation. As noted before, however, we are now allowing the optimizer freedom to design gaps or interference fits in the mechanism.

A close inspection of Fig. 13 shows that the new design has an intentional interference fit, and the force deflection curve has been shifted to the left due to the initial assembly deflection that results from the interference. The interference can be recognized in Fig. 13a by the intersection of the cam surface and the optimized geometry. It is important to note that according to the contact mechanics approach presented in Section 3.1, springs experiencing an interference are deflected in the negative deflection direction as if the spring were being assembled into a housing comprising the cam. This assembly pushes the spring into a position where the cam and the spring are in contact but not interfering. This assembly deflection and the corresponding residual stresses are used as an initial condition when we apply the total deflection. Since we use the same operational displacement range, the intentional interference results in a larger applied preload. This means that the force must remain constant over a smaller portion of the entire deflection range, and therefore more constant-force designs can be found.

After the optimization is complete, we use the same Monte Carlo simulation that we used in the previous section to check the robustness of the solution; the histogram is shown in Fig. 10c. We see from the histogram that the designs are clustered within a small region of variation and that they have a desirable constant force percentage. The average constant force percentage is 97.64%, with a standard deviation of 0.76%. We see that the new design improves both the average percentage and the standard deviation. As described in the previous paragraph, we attribute the improvement in average percentage to allowing the optimizer the freedom to intentionally design gaps or interference fits in the mechanism. Additionally, we

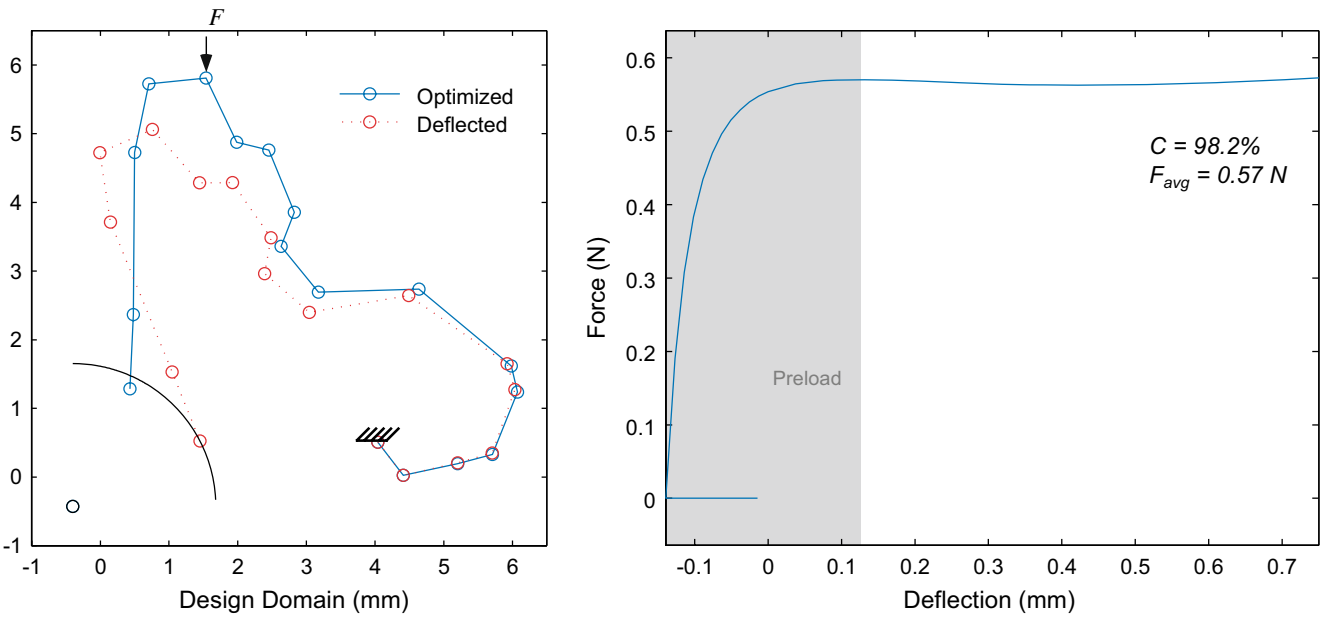

Fig. 13 Case 2 Robust design solution: (**a**) Side view of optimized geometry (nodal representation) with non exaggerated deflected shape; (**b**) Force deflection curve for optimized design.

attribute the improvement in robustness to the formulation of the optimization objective function, which seeks to improve the constant force percentage for the nominal geometry *and* seeks to reduce its variation in the presence of known manufacturing tolerances. Notice that all previous studies considered only the nominal geometry case.

Before concluding we must also verify that our robust design optimization solution does not violate our constraints when manufactured within our tolerances. The Monte Carlo simulation used earlier is also used to evaluate the constraints for a sample of contacts. The results confirmed that the original, or unadjusted, constraints are not violated.

5 Concluding remarks

In this paper we have presented a new design strategy for the design optimization of constant-force electrical contacts, which are small scale springs that conduct electricity. This approach presented in this paper provides more freedom for the optimization than the model used in previously published work (Weight et al. 2007) by giving individual nodes complete freedom to relocate within the design domain, and by allowing the optimizer to consider intentional gaps and interferences in the mating of emulated pin-joints. The implementation of the improved approach resulted in a significant increase in percentage of constant force. Using the previously published approach a deterministic design was found with 73.20% constant force, a value that was increased to 97.50% by using the new model.

We also presented manufacturing uncertainties that may be encountered when producing constant-force-electrical contacts, and explored specific situations that may alter the mating condition of the contact parts. To control these situations we developed a new model of the contact, and formulated a design optimization problem that not only reduced the variation in performance, but increased the performance to 98.20% constant force. This was made possible by allowing the optimizer to intentionally design for gaps and interference fits. It is worth noting that it is completely possible to design and then manufacture these intentional interferences; many connector systems are preloaded using intentional interferences between mating parts. This is done by adjusting assembly fixtures so that

Table 5 Comparison of the benchmark, case 1, and case 2 designs, with 1,000 Monte Carlo simulation samples (see Table 6 for results based on 10,000 samples)

	Benchmark	Case 1 (Deterministic)	Case 2 (Robust)
Percent constant force	73.20%	97.50%	98.20%
Average percent constant	70.24%	94.82%	97.64%
Standard deviation	1.68%	2.46%	0.76%

Table 6 Comparison of the benchmark, case 1, and case 2 designs, with 10,000 Monte Carlo simulation samples

	Benchmark	Case 1 (Deterministic)	Case 2 (Robust)
Average percent constant	70.55%	94.61%	97.38%
Standard deviation	1.90%	2.60%	0.86%

the placement of the spring in relation to the housing results in desired interference.

A Monte Carlo simulation has verified that the design identified by the robust design optimization performed as expected. The average percentage constant force for the robust design is 97.64% with a standard deviation of 0.76%. This can be compared to the Monte Carlo results from the deterministic optimization, 94.82% constant with a standard deviation of 2.46%. Table 5 gives a summary of the comparison between these three designs using 1,000 samples in the Monte Carlo simulation, while Table 6 presents results for 10,000 samples. Table 6 is provided to show that for the mechanism models presented in this paper, 1,000 samples is a reasonable number of samples to use, especially when considering the additional computational expense that accompanies the use of more samples.

Acknowledgements The authors gratefully acknowledge the support of the Fulton College of Engineering and Technology at Brigham Young University for their support of this project. The authors also thank ATL Technology for their practical insight on electrical connector design, which was generously shared with the authors.

References

Bhatti M (2006) Advanced topics in finite element analysis of structures. John Wiley and Sons, Ch 7

Chen W, Wiecek MM, Zhang J (1999) Quality utility - a compromise programming approach to robust design. ASME J Mech Des 121:179–187

Chen W, Sahai A, Messac A, Sundaraj GJ (2000) Exploring the effectiveness of physical programming in robust design. ASME J Mech Des 122(2):155–163

Choi JH, Lee SJ, Choi DH (1998) Stochasitic linkage modeling for mechanical error analysis of planar mechanisms. Mechan Struct Mach 26(3):257–276

DeVor RE, Chang T-H, Sutherland JW (1992) Statistical quality design and control: contemporary concepts and methods. Prentice Hall, New Jersey, pp 525–535

Evans MS, Howell LL (1999) Constant-force end-effector mechanism. In: Proceedings of the IASTED international conference, robotics, and applications, pp 250–256

Frischknecht BD, Howell LL, Magleby SP (2004) Crank-slider with spring constant force mechanism. In: Proceedings of the ASME design engineering technical conferences, DETC-2004-MECH-57318

Garrett RE, Hall AS (1969) Effect of tolerance and clearance in linkage design. ASME J Eng Ind 91(1):198–202

Herder JL, van den Berg FPA (2000) Two spatially balanced compliant mechanisms (SBCM's), an example and prospectus. In: Proceedings of the ASME design engineering technical conferences, DETC-2000-MECH-14120

Howell LL (2001) Compliant mechanisms. John Wiley & Sons, New York, NY

Howell LL, Magleby SP (2006) Substantially constant-force exercise machine. Patent No. US 7,060,012 B2

Jenuwine JG, Midha A (1994) Synthesis of single-input and multiple-output port mechanisms with springs for specified energy absorption. ASME J Mech Des 116(3):937–943

Koch PN (2002) Probabilistic design: optimizing for six sigma quality. In: AIAA 43rd AIAA/ASME/ASCE/AHS structures, structural dynamics, and materials conference, Paper Number AIAA–2002–1471

Murphy MD, Midha A, Howell L (1996) The topological synthesis of compliant mechanisms. Mech Mach Theory 31(2): 185–199

Nathan RH (1985) A constant force generation mechanism. ASME J Mech Transm Autom Des 107:508–512

Nahar DR, Sugar T (2003) Compliant constant-force mechanism with a variable output for micro/macro applications. In: Proceedings of IEEE international conference on robotics and automation, vol 1, pp 318–323

Parkinson MB, Howell LL, Cox JJ (1997) A parametric approach to the optimization-based design of compliant mechanisms. In: Proceedings of the ASME design engineering technical conferences, DETC-1997-DAC-3763

Parkinson A, Sorensen C, Pourhassan N (1993) A general approach for robust optimal design. ASME J Mech Des 115: 74–80

Su J, Renaud JE (1997) Automatic differentiation in robust optimization. AIAA J 35(6):1072–1079

Taguchi G (1986) Introduction to quality engineering. Krauss International Publications, White Plains, NY

Weight BL (2001) Development and design of constant-force mechanisms. Master's thesis, Department of Mechanical Engineering, Brigham Young University, Provo, UT

Weight BL, Magleby SP, Howell LL (2002) Selection of compliant constant-force mechanisms based on stress and force criteria. In: Proceedings of the ASME design engineering technical conferences, DETC-2002-MECH-34206

Weight BL, Mattson CA, Magleby SP, Howell LL (2007) Configuration selection, modeling, and preliminary testing in support of constant force electrical connectors. ASME J Electron Packag 129(3):236–246